Earth and Planetary Science Letters 481 (2018) 305–315

Contents lists available at ScienceDirect

Earth and Planetary Science Letters

www.elsevier.com/locate/epsl

Carbon dioxide generation and drawdown during active orogenesis of siliciclastic rocks in the Southern Alps, New Zealand

Catriona D. Menzies [a,*], Sarah L. Wright [a], Dave Craw [b], Rachael H. James [a], Jeffrey C. Alt [c], Simon C. Cox [d], Iain K. Pitcairn [e], Damon A.H. Teagle [a]

[a] Ocean and Earth Science, National Oceanography Centre Southampton, University of Southampton, Southampton, SO14 3ZH, UK
[b] Department of Geology, University of Otago, Dunedin 9016, New Zealand
[c] Department of Earth and Environmental Science, The University of Michigan, 1100 North University Avenue, Ann Arbor, MI 48109-1005, USA
[d] GNS Science, Private Bag 1930, Dunedin 9054, New Zealand
[e] Department of Geological Sciences, Stockholm University, SE-10691 Stockholm, Sweden

ARTICLE INFO

Article history:
Received 12 May 2017
Received in revised form 23 September 2017
Accepted 6 October 2017
Available online xxxx
Editor: M. Bickle

Keywords:
CO_2
mountain building
carbon isotopes
metamorphism
carbon cycle
chemical weathering

ABSTRACT

Collisional mountain building influences the global carbon cycle through release of CO_2 liberated by metamorphic reactions and promoting mechanical erosion that in turn increases chemical weathering and drawdown of atmospheric CO_2. The Southern Alps is a carbonate-poor, siliciclastic mountain belt associated with the active Australian Pacific plate boundary. On-going, rapid tectonic uplift, metamorphism and hydrothermal activity are mobilising carbon. Here we use carbon isotope measurements of hot spring fluids and gases, metamorphic host rocks, and carbonate veins to establish a metamorphic carbon budget. We identify three major sources for CO_2 within the Southern Alps: (1) the oxidation of graphite; (2) consumption of calcite by metamorphic reactions at the greenschist–amphibolite facies boundary, and (3) the dissolution of groundmass and vein-hosted calcite. There is only a minor component of mantle CO_2 arising on the Alpine Fault. Hot springs have molar HCO_3^-/Ca^{2+} ~9, which is substantially higher than produced by the dissolution of calcite indicating that deeper metamorphic processes must dominate.
The total CO_2 flux to the near surface environment in the high uplift region of the Southern Alps is estimated to be $\sim 6.4 \times 10^8$ mol/yr. Approximately 87% of this CO_2 is sourced from coupled graphite oxidation (25%) and disseminated calcite decarbonation (62%) reactions during prograde metamorphism. Dissolution of calcite and mantle-derived CO_2 contribute ~10% and ~3% respectively. In carbonate-rich orogens CO_2 production is dominated by metamorphic decarbonation of limestones. The CO_2 flux to the atmosphere from degassing of hot springs in the Southern Alps is 1.9 to 3.2×10^8 mol/yr, which is 30–50% of the flux to the near surface environment. By contrast, the drawdown of CO_2 through surficial chemical weathering ranges between 2.7 and 20×10^9 mol/yr, at least an order of magnitude greater than the CO_2 flux to the atmosphere from this orogenic belt. Thus, siliciclastic mountain belts like the Southern Alps are net sinks for atmospheric CO_2, in contrast to orogens involving abundant carbonate rocks, such as the Himalaya, that are net CO_2 sources.
© 2017 The Author(s). Published by Elsevier B.V. This is an open access article under the CC BY license (http://creativecommons.org/licenses/by/4.0/).

1. Introduction

Collisional mountain belts may have been significant sources and/or sinks of atmospheric CO_2 over geological time through the generation of CO_2 in metamorphic reactions and drawdown of CO_2 during enhanced chemical weathering of silicates. Uplift of the Himalaya and Tibetan plateau and resulting enhanced weathering over the past 40 Myr has been attributed as a driving force for global late Cenozoic cooling (Raymo and Ruddiman, 1992), and orogenic cycles have undoubtedly influenced the global carbon cycle (Bickle, 1996), but the balance between CO_2 drawdown and release is poorly constrained and the overall effect results from variations in local climate, tectonic setting, rock type, and duration of the mountain building.

Active orogenic belts are estimated to currently be adding equivalent amounts of CO_2 to that from volcanoes (Kerrick et al., 1995; 0.7 to 3.5×10^{12} mol/yr of CO_2 from mid ocean ridges, and 1.5–3.6×10^{12} mol/yr from volcanic arcs, Kelemen and Manning, 2015). The presence of metamorphic calc-silicate minerals in high grade rocks and abundant limestones in many orogenic belts, such as the North American Cordillera, the Himalaya, the

* Corresponding author.
E-mail address: c.menzies@soton.ac.uk (C.D. Menzies).

https://doi.org/10.1016/j.epsl.2017.10.010
0012-821X/© 2017 The Author(s). Published by Elsevier B.V. This is an open access article under the CC BY license (http://creativecommons.org/licenses/by/4.0/).

European Alps, and numerous portions of the SW Pacific Rim in Indonesia and New Guinea, is evidence that orogenic CO_2 is mainly generated by metamorphic decarbonation as described by the simplified Ca-endmember reaction: limestone + quartz = wollastonite + CO_2. In the Himalaya high grade decarbonation reactions produce abundant CO_2, most (~70%) of which migrates to the surface via thermal springs (0.9×10^{12} mol CO_2/yr for the Himalayan orogen; Becker et al., 2008; Evans et al., 2008).

Active tectonics, steep slopes, and orographic effects mean that mountain belts are sites of rapid physical erosion. The resulting comminution and generation of fresh mineral surfaces can lead to elevated rates of chemical weathering. Weathering of calcium silicates generates a sink for CO_2 through reactions of the form: $2CO_2 + 3H_2O + CaAl_2Si_2O_8$ (anorthite) $\rightarrow Ca^{2+} + Al_2Si_2O_5(OH)_4$ (kaolinite) $+ 2HCO_3^-$ where two moles of CO_2 are drawn down during weathering reactions although one mole is subsequently released if the precipitation of marine carbonates occurs (Brady, 1991). The effectiveness of such silicate weathering reactions and net drawdown of CO_2 remain debated, but the best estimate of CO_2 removal rate for the present day is $\sim 11.7 \times 10^{12}$ mol CO_2/yr by silicate weathering and $\sim 24 \times 10^{12}$ mol CO_2/yr total including carbonate weathering (Gaillardet et al., 1999). Approximately 0.27×10^{12} mol CO_2/yr is drawn down through weathering reactions in the Himalayan Ganges–Brahmaputra basin (Galy and France-Lanord, 1999), a factor of three to four lower than the estimated release from metamorphic reactions in this region (Becker et al., 2008; Evans et al., 2008).

In contrast, some active mountain belts, such as in Taiwan and the Southern Alps, New Zealand, contain relatively few carbonate rocks and comprise siliciclastic metasediments with low carbon contents (<2 wt.% C, Pitcairn et al., 2006). These rocks contain carbon as variably matured organic debris, and metamorphic interstitial carbonate and veins. However, CO_2-effusing warm springs are also common in these mountain belts (Barnes et al., 1978; Upton et al., 2011). The contribution of these low-carbon rocks to the global CO_2 budget is poorly constrained and likely to be small. Nevertheless, the crustal processes that generate this CO_2 in low-carbon orogenic belts are of interest, as they may also be operating in the major carbonate-bearing mountain chains but are obscured by the overwhelming supply of limestone-derived CO_2. The proportion of the total metamorphic CO_2 flux these processes constitute will depend on the mineralogy and organic carbon content of the metamorphic pile. In this paper, we evaluate the potential deep sources for CO_2 in the active low carbon orogen of the Southern Alps, New Zealand. We define the relative contributions of different key metamorphic reactions, and provide estimates of the likely fluxes of CO_2 to the surface environment from the various deep sources within the active mountain belt. This flux is then compared with estimates of CO_2 drawdown through weathering for this area to estimate the net CO_2 balance for a siliciclastic orogenic belt.

1.1. Geological and tectonic setting

The South Island of New Zealand lies astride the Pacific-Australian plate boundary, and is being deformed by oblique dextral collision of these plates (Cox and Sutherland, 2007). The basement rocks are Paleozoic–Mesozoic siliciclastic metasedimentary rocks that were variably metamorphosed in the Mesozoic during terrane accretion on the margin of Gondwana (Mortimer, 2004). Since the onset of convergence along this plate boundary in the Miocene (Sutherland et al., 2000), these basement rocks are being redeformed and metamorphosed to amphibolite facies as they pass through the modern orogen in a 5 km thick zone beneath the Southern Alps (Pitcairn et al., 2014).

The metasedimentary rocks are being uplifted to form the >3000 m Southern Alps orogenic belt on the hangingwall of the Alpine Fault, the main plate boundary structure (Cox and Sutherland, 2007). Long-term, multiple-earthquake, uplift rates vary from >8 mm/yr adjacent to the Alpine Fault, to <1 mm/year in the high mountains (Main Divide region) and their eastern slopes (Outboard Zone, Fig. 1) (Norris and Cooper, 2007; Teagle et al., 1998). Erosion rates in the Inboard Zone near the Alpine fault are similar to uplift rates, so that the western slopes of the mountains retain a near steady state topographic profile, and upper greenschist to amphibolite facies metasediments are being rapidly exhumed from the middle crust (Koons, 1989). This rapid exhumation results in a high geothermal gradient, with temperatures of 350 °C as shallow as 6–8 km (Koons, 1987). Consequently the brittle-ductile transition has been raised from a regional normal of 10–12 km to form a shallow base to the seismogenic zone at ~8–10 km depth (Boese et al., 2012).

The high mountains and their eastern slopes consist of low grade (greenschist facies and lower) Mesozoic metasediments that are dominated by metagreywackes (lithic sandstones) with interlayered meta-argillites and minor metabasites (Cox and Barrell, 2007; Grapes and Watanabe, 1992) that are lithologically and geochemically similar to the high grade rocks that are being exhumed along the Alpine Fault (Fig. 1).

The principal slip zone of the Alpine Fault acts as a barrier to cross fault fluid flow throughout the crust (Menzies et al., 2016; Sutherland et al., 2012) and combined with the steep topography and the high geothermal gradient results in geothermal circulation in the Alpine Fault hangingwall (Menzies et al., 2016). Hot springs occur in deeply-incised valleys up to 17 km east of the Alpine Fault and deeper fluid flow causes deposition of hydrothermal veins from the near-surface to the middle crust (Fig. 1) (Menzies et al., 2014). The hot spring fluids commonly effervesce CO_2, and trapped metamorphic fluids studied in fluid inclusions in quartz veins contain abundant CO_2 (up to 5 mol% end member fluid, Craw and Norris, 1993).

2. Methods

To investigate the behaviour of carbon in the Southern Alps orogenic belt, we have analyzed basement rock samples spanning an exhumed crustal cross section from prehnite–pumpellyite facies to garnet–oligoclase amphibolite facies for total carbon content, total organic carbon and carbonate content, $\delta^{13}C$ values of organic carbon/graphite and $\delta^{13}C$ values of active geothermal fluids and calcite veins throughout the crust. This study has made use of a well chararacterised collection of rock samples taken from the full suite of metamorphic grades through the Mesozoic and Cenozoic orogens (Pitcairn et al., 2006). Samples were obtained from fresh outcrops in road cuts and river gorges. Samples of Cenozoic calcite-bearing veins were collected from amphibolite facies rocks in river gorges and glaciated exposures near the Alpine Fault (Menzies et al., 2014).

Spring waters were collected following Menzies et al. (2016) and river waters were sampled following the same protocols, although alkalinity titrations were carried out using 0.01 N HNO_3. Major cations in river water samples were analyzed by a Perkin Elmer Optima 4300 DV ICP-OES at the National Oceanography Centre Southampton following Menzies et al. (2016). Precision and accuracy were assessed using internal reference solution SLRS4 and in-house reference solution Sco2/15 resulting in precision better than 7% and accuracy better than 6%.

Total carbon contents and total organic carbon contents were analyzed on bulk rock powders on an elemental analyzer (EA). Traces of carbonate C were removed by reaction with dilute (3N) HCl, followed by washing in distilled H_2O (Könitzer et al., 2012).

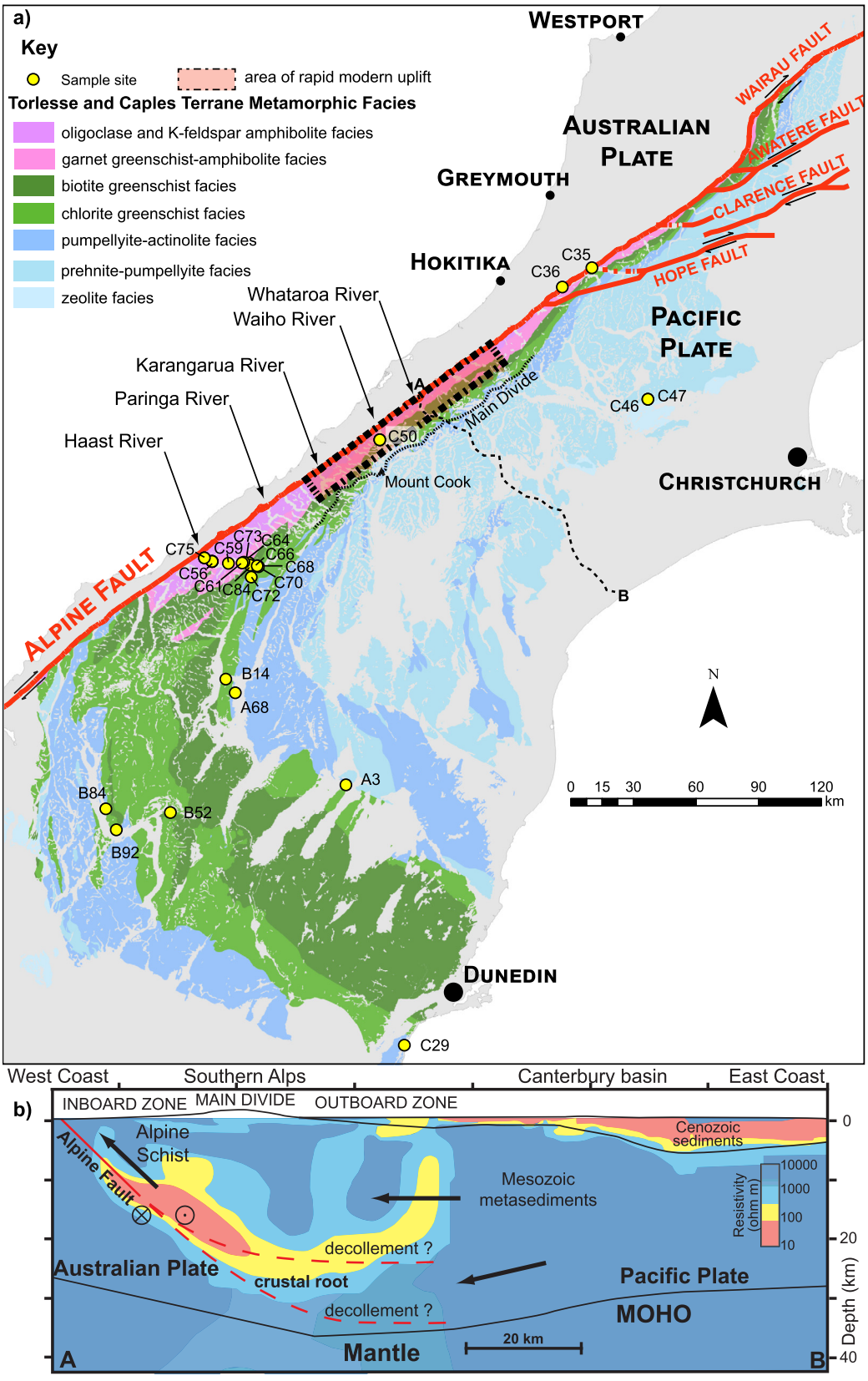

Fig. 1. a) Geological map of South Island, New Zealand coloured by metamorphic grade of the Haast Schist. Sample locations and numbers are marked. Dashed line indicates location of resistivity cross section in part b and shaded dashed box outlines the area of modern day rapid uplift. b) Cross section of central South Island along dashed line A to B from Menzies et al. (2016). Zone of active metamorphism is shown as a "crustal root" beneath the orogen and down dip of the resistivity anomaly.

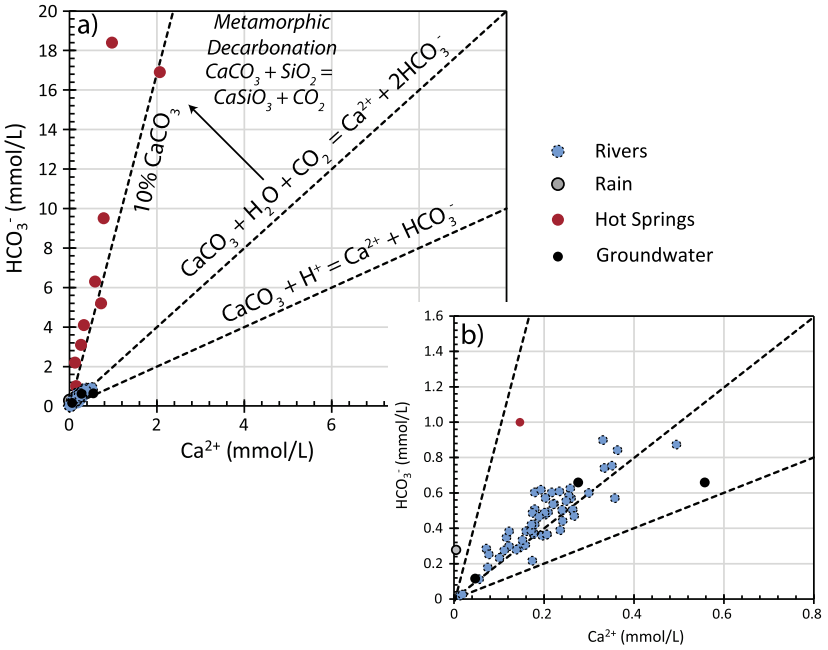

Fig. 2. a) HCO_3 versus Ca molal contents in spring waters lie above the calcite dissolution trend lines indicating loss of Ca or addition of CO_2 from another source with only 10% attributed to dissolution of $CaCO_3$. b) Larger scale view of river water, groundwater and rainwater in relation to $CaCO_3$ dissolution trends. Hot Spring data from Menzies et al. (2016).

The $\delta^{13}C$ of TOC and TC were determined at the University of Michigan with a Costech EA coupled to a Thermo Scientific Delta V plus isotope ratio MS (IRMS), using IAEA 600 Caffeine ($\delta^{13}C = -27.77‰$ VPDB) and IAEA-CH-6 Sucrose ($-10.45‰$) as calibration standards. Rock powders were degassed at 100 °C and stored under vacuum to minimize adsorption of atmospheric CO_2. Replicate analyses of low-C content samples (<500 ppm) were within ±70 ppm and ±0.5‰ $\delta^{13}C$. Carbon blanks are less than 6% of reported C contents.

3. Results

3.1. Carbon in river and spring waters

River waters and shallow recharge groundwaters typically contain 123 to 899 µmol/L dissolved HCO_3^- (Table S1) and show a 2:1 relationship between dissolved HCO_3^- and Ca^{2+} that reflects calcite dissolution that involves atmospheric CO_2 as carbonic acid (Fig. 2). This trend is distinctly different from one which involves calcite dissolution via acid reactions that is typical of deeper groundwaters and has a 1:1 molar relationship (Fig. 2). In contrast, spring waters show a strong trend towards high dissolved HCO_3^-, ranging up to 19,000 µmol/L at relatively low Ca^{2+} concentrations (Fig. 2A, Menzies et al., 2016). The dissolved carbon concentrations of these springs are minima because many effervesce of CO_2 and precipitate calcite as they upwell. The abundant rain on the west side of the mountains contains low concentrations of dissolved carbon (<20 µmol/L HCO_3^-, Fig. 2; Cox et al., 2015; Jacobson et al., 2003).

When carbon is released during metamorphic decarbonation reactions the molar HCO_3^-/Ca^{2+} ratio of the resulting metamorphic fluids would be significantly greater than 2 as CO_2 is released from carbonates and Ca sequestered in calcium silicates (Fig. 2). The high HCO_3^-/Ca^{2+} ratios of warm springs in the Southern Alps (7–19) may indicate that decarbonation reactions are occurring even though carbonate is a minor component of the rock mass.

3.2. Rock organic carbon contents and isotope compositions

The total organic carbon (TOC) contents of the rocks are typically <0.3 wt.% at all metamorphic grades, although our data suggest that the upper greenschist and amphibolite facies rocks have slightly lower TOC contents than lower grade rocks (Fig. 3a), but the difference is insignificant above 72% confidence levels. Organically derived graphitic carbon occurs in a wide range of textures across the spectrum of metamorphic grades formed during the Mesozoic (Beyssac et al., 2016). In the lowest grade rocks, the carbonaceous material is typically irregularly shaped 1–10 µm particles distributed through the relict sedimentary rock textures (Hu et al., 2015). FT-IR spectra identify significant less-well ordered kerogen in carbonaceous material from unmetamorphosed greywacke to Greenschist Facies schist (Pitcairn et al., 2005). Carbonaceous material also occurs in rocks of higher metamorphic grade and in general most of this material is more mature with fewer short chain hydrocarbons, although carbonaceous material from some Amphibolite Facies Alpine Schist retain immature kerogen as shown by FT-IR spectra (Pitcairn et al., 2005). The presence of immature hydrocarbons in carbonaceous material at greenschist and amphibolite facies may facilitate oxidation of rock mass carbon. Several studies have shown carbonaceous material from such metamorphic facies display evidence of graphite remobilisation in ductile and brittle shear structures (Henne and Craw, 2012; Hu et al., 2015; Kirilova et al., in press; Pitcairn et al., 2005).

The $\delta^{13}C$ values of the graphitic material range between -29.5 and $-17.2‰$ (Table 1; Fig. 4). As inferred Mesozoic metamorphic temperatures of the rocks increase, the $\delta^{13}C$ values of the graphitic material in the rocks also increase, from $-26.1‰$ (average, $n = 6$) in low grade to prehnite–pumpellyite facies rocks to $-20.4‰$ (average, $n = 8$) in upper greenschist and amphibolite facies rocks. Rayleigh distillation calculations suggest that the carbonaceous material matured during the Mesozoic metamorphism by CH_4 production as opposed to CO_2 loss (Fig. 4). Upper greenschist facies graphitic material entering the Cenozoic Southern Alps orogen has $\delta^{13}C = -22.5$ to $-20.3‰$ and the resulting amphibolite facies schists exhumed adjacent to the Alpine Fault have

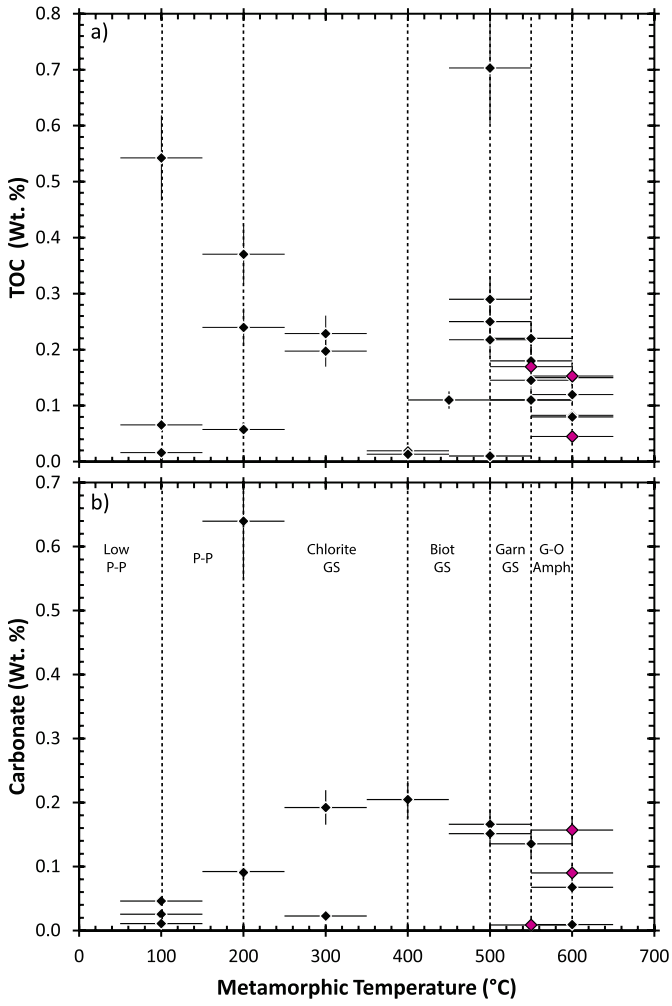

Fig. 3. a) Total organic carbon (TOC) content versus rock metamorphic temperature shows a general decrease in TOC as metamorphic temperature increases, but the difference is insignificant above 72% confidence levels as there is significant scatter in the data. b) Carbonate content versus metamorphic temperature, no trend observed. Coloured diamonds in each plot are data from the Alpine Fault. Low P–P: Low Prehnite–Pumpellyite Facies; P–P: Prehnite–Pumpellyite Facies; Chlorite GS: Chlorite Greenshist Facies; Biot GS: Biotite Greenschist Facies; Garn GS: Garnet Greenschist Facies; G–O Amph: Garnet–Oligoclase Amphibolite Facies. (For interpretation of the references to color in this figure legend, the reader is referred to the web version of this article.)

graphitic material with $\delta^{13}C$ values ranging between −22.0 and −18.5‰ ($n = 4$) (Fig. 4).

3.3. Calcite contents and carbon isotope composition

Calcite is a minor constituent of the rock mass in the Southern Alps and commonly occurs in veins (Jenkin et al., 1994; Menzies et al., 2014). The carbonate concentration of the rocks does not vary significantly across metamorphic grades (Fig. 3b), the difference is insignificant above 50% confidence levels. In the modern orogen, this calcite was remobilised in the Alpine Fault hangingwall, and calcite is found as a vein mineral from the brittle to ductile transition zone to the near surface in the Alpine Fault Zone and extends further east into the Main Divide (Menzies et al., 2014). This calcite precipitated at a wide range of temperatures and depths (<1 km to >6 km depth) (Jenkin et al., 1994; Menzies et al., 2014).

Mesozoic metamorphic calcite has $\delta^{13}C$ values ranging between −11 and −6‰ (Templeton et al., 1998), in equilibrium with CO_2 having $\delta^{13}C$ values of −9.7 to −4.7‰ at 250 °C (using fractionation equation of Bottinga (1968)). In the Alpine Fault Zone the $\delta^{13}C$ values of CO_2 in equilibrium with calcite range between −10.1 and −3.8‰ (Fig. 5). Modern day hot springs in the Southern Alps have $\delta^{13}C_{DIC}$ values ranging between −16.8 and −5.7‰ with an average of −9.1 ± 4‰ (Fig. 5, Menzies et al., 2016), indicating CO_2 in the springs and Cenozoic veins may be in part derived from the remobilisation of Mesozoic calcite (Fig. 5). However, high HCO_3^- to Ca^{2+} ratios in the springs (Fig. 2) preclude calcite dissolution being the sole source for CO_2, unless significant calcium is removed by metamorphic reactions. An alternative would be the shallow precipitation beneath the springs of secondary non-carbonate calcium minerals, but this has not been observed.

4. Discussion

4.1. Metamorphic reactions producing CO_2 in Alpine Schist

The principal reactions involving Ca-bearing phases that occur in the Alpine orogenic metamorphism from greenschist to amphibolite facies schist are the formation of oligoclase and breakdown of epidote and replacement of titanite by ilmenite (eq. (2)) (Grapes and Watanabe, 1992). Either or both of the two carbon-bearing minerals, graphite and calcite, may be involved in reactions at this metamorphic transition, but modal changes must be small as their abundances are statistically similar in both greenschist facies rocks and amphibolite facies hangingwall schists next to the Alpine Fault (Table 1; Fig. 3). Hence, we restrict our calculations to <10% calcite and/or graphite loss (see mass balance below, Table 2).

Dissolved oxygen in metamorphic fluids near the greenschist-amphibolite facies transition, in the presence of graphite, is negligible, with log $fO_2 \sim -45$ (calculated using Geochemist's Workbench). Consequently, oxidation of graphite requires redox reactions that do not involve free oxygen. The reduction of epidote ferric iron to ferrous iron-bearing ilmenite provides a potential redox partner for the oxidation of graphite. Greenschist facies quartzofeldspathic schist contains ~4 wt.% epidote and minor greenschist facies metabasic schist contains ~10 wt.% epidote (Grapes and Watanabe, 1992). This epidote is typically Ps = 20 at greenschist facies, so contains ~6 wt.% Fe^{3+} (Grapes and Watanabe, 1992).

CO_2 generated during such reactions at the greenschist-amphibolite facies transition (at ~550 °C) would have $\delta^{13}C$ values of −14.4 to −7.8‰ which is similar to the range of recorded $\delta^{13}C_{DIC}$ values in spring waters (−16.8 to −5.7‰), and to $\delta^{13}C$ values of CO_2 in equilibrium with calcite veins (−11.7 to −3.8‰) (Fig. 5).

Metamorphic decarbonation of calcite is the other principal potential source of metamorphic CO_2 (Table 2). Quartzofeldspathic schist is calcium-poor, typically containing ~2 wt.% CaO (Pitcairn, 2004). In greenschist facies rocks, Ca is present as calcite (~1–5 modal %), epidote (~4%) and titanite (~1–2%), with rare actinolite. Prograde metamorphism to amphibolite facies in the Alpine orogen generates (~20%) oligoclase of An_{20} from the breakdown of epidote and titanite and replacement of albite. This reaction may also involve the breakdown of calcite (Grapes and Otsuki, 1983) consuming Ca and releasing CO_2. Minor metabasic schists have ~10 wt.% CaO and undergo similar mineralogical changes at the greenschist to amphibolite facies transition, although they have a greater proportion of epidote (10%) which breaks down to form hornblende (20%) and oligoclase (20%) at amphibolite facies.

4.2. Mass balance at the greenschist to amphibolite facies transition

The greenschist to amphibolite facies metamorphic transformation may facilitate the release of CO_2, whilst consuming Ca, in order to satisfy the elevated HCO_3^-/Ca ratios measured in modern day spring waters. This can be summarised with the following

Table 1
Summary of carbon content and carbon isotope ratios of carbonaceous material in Southern Alps metasediments. $CaCO_3$ contents were determined by difference between Total Carbon (TC) and Total Organic Carbon (TOC) and rounding errors result in discrepancies where $CaCO_3$ + TOC to not exactly equal TC.

Sample no.	GR_E	GR_N	Locality	Lith.	Met. Grade	Met. T (°C)	TOC (wt.%)	TC (wt.%)	$CaCO_3$ wt.%	$\delta^{13}C_{graphite}$ (‰)
C46	2409656	5766383	Porters Pass	GW	Low P–P	100	0.07	0.09	0.03	−26.2
C47	2409656	5766383	Porters Pass	GW	Low P–P	100	0.02	0.06	0.05	−26.1
C29	2293000	5457500	Taieri	Pel	Low P–P	100	0.54	0.55	0.01	−22.1
A68	2212000	5626000	Hawea	Pel	P–P	200	0.37	1.01	0.64	−25.0
A3	2265000	5582000	Oturehua	Pel	P–P	200	0.24	0.33	0.09	−27.4
B84	2150000	5570500	Glenorchy	Pel	P–P	200	0.06	0.15	0.09	−29.5
B14	2207500	5632500	Hawea	Pel	Chlor GS	300	0.23	0.42	0.19	−22.3
B92	2155000	5560500	Glenorchy	Pel	Chlor GS	300	0.20	0.22	0.07	−24.1
B52	2180900	5568700	Remarks	Psam	Chlor GS	400	0.02	1.07	1.05	−22.5
C72	2219700	5681300	Pleasant Flat	QFS	Chlor GS	400	0.01	0.22	0.20	−25.5
C68	2222900	5686500	Haast	QFS	Biot GS	500	0.70	0.87	0.17	−21.0
C35	2382844	5829246	Rocky Point	QFS	Biot GS	500	0.22	0.37	0.15	−21.7
C64	2218700	5688100	Haast	QFS	Garn GS	550	0.15	0.28	0.14	−17.2
C50	2281204	5746989	Haast	QFS	Garn GS	550	0.17	0.18	0.01	−21.0
C59	2208700	5687900	Haast	QFS	G–O Amph	600	0.12	0.13	0.01	−21.1
C56	2200900	5688800	Haast	QFS	G–O Amph	600	0.08	0.15	0.07	−19.6
C75	2197200	5690500	Haast – AF	QFS	G–O Amph	600	0.04	0.14	0.09	−18.5
C36	2368700	5820000	Northern – AF	PM	G–O Amph	600	0.15	0.31	0.16	−22.0
C70*	2223100	5686300	Haast	QFS	GS – Chlor	450	0.11	nd	nd	−22.5
C84*	2219200	5687000	Haast	QFS	GS – Biot	500	0.25	nd	nd	−20.3
C73*	2216100	5688400	Haast	MB	GS – Biot	500	0.01	nd	nd	−26.2
C66*	2222500	5686700	Haast	QFS	GS – Biot	500	0.29	nd	nd	−22.5
C76*	2200900	5688800	Haast	QFS	GS – Garn	550	0.11	nd	nd	−23.9
C77*	2200900	5688800	Haast	QFS	GS – Garn	550	0.11	nd	nd	−21.6
C50*	2281204	5746989	Franz Josef – AF	QFS	GS – Garn	550	0.22	nd	nd	−21.2
C61*	2215300	5688100	Haast	QFS	GS – Garn	550	0.18	nd	nd	−18.9
C56*	2200900	5688800	Haast	QFS	G–O Amph	600	0.15	nd	nd	−20.4
C75*	2197200	5690500	Haast – AF	QFS	G–O Amph	600	0.08	nd	nd	−19.3

Notes: GW = Greywacke, Pel = Pelite, Psam = Psammite, QFS = Quartzofeldspathic Schist, PM = Protomylonite, MB = metabasite. Low P–P = Low prehnite pumpellyite, P–P = Prehnite pumpellyite, Chlor GS = Chlorite Greenschist, Biot GS = Biotite Greenschist, Garn GS = Garnet Greenschist, G–O Amph = Garnet Oligoclase Amphibolite. nd = not determined, AF = Alpine Fault Lith. = lithology of the sample, Met. Grade = Metamorphic grade of the sample, Met T. = Estimated maximum metamorphic temperature the sample experienced. Samples with an * are from Hilton et al. (2008).

Table 2
Summary of changes in mineralogy at the greenschist to amphibolite facies transition and associated reactions that generate CO_2 based on mineral proportions outlined in eq. (2) and consuming no more than 10% of the carbon-bearing minerals. Changes in mineralogy match whole rock geochemistry data collected by Pitcairn (2004).

Example rocks	Greenschist		Amphibolite		
	wt.%	Moles	wt.%	Moles	%Ca
Epidote, pS20	4.4	0.667	0	0	9.4
Albite	21.5	5.3	0	0	
Calcite	3.1	2	2.8	1.8	40
Graphite	0.21	0.017	0.2	0.016	
Titanite	0.9	0.3	0	0	20.3
Quartz	18.6	20	18.6	20	
Muscovite	24.7	2	24.7	2	
Chlorite	27.0	2.7	0.0	0	
Oligoclase, An20	0.0	0	23.8	5.8	
Ilmenite	0.0	0	0.7	0.3	
Biotite	0.0	0	29.3	2	
	100.5		100.2		
Oligoclase formation:			**Redox:**		
Oligoclase, Ca	0.72	Ca, wt.%	Epidote > Ilmenite + O_2	0.3	Fe^{3+}, wt.%
Titanite (Ti)	0.19	Ca, wt.%	(6% Fe)	0.0047	Fe^{3+}, mol
Epidote (Ep)	0.41	Ca, wt.%	Oxygen available	0.0024	O, mol
Total Ca from Ep, Ti	0.60	Ca, wt.%		0.001	CO_2, mol
Ca required from $CaCO_3$	0.12	Ca, wt.%	CO_2 liberated from graphite	0.05	CO_2, wt.%
	0.003	Ca, mol	Total CO_2	**0.18**	CO_2, g
CO_2 liberated, $CaCO_3$	0.13	CO_2, g		**4.2**	CO_2, mmol

reaction that includes the major components in appropriate proportions (based on measured mineral modes) that consumes minor amounts of both calcite and graphite:

$$\begin{aligned} &5.3NaAlSi_3O_8\,(\text{Albite}) + 0.3CaTiSiO_5\ (\text{Titanite}) \\ &\quad + 0.7CaAl_{2.55}Fe_{0.45}Si_3O_{12}(OH)\ (\text{Epidote}) \\ &\quad + 0.2CaCO_3\,(\text{Calcite}) + 0.08C\ (\text{Graphite}) \\ &\quad = 5.83Na_{0.8}Ca_{0.2}Al_{1.2}Si_{2.8}O_8\ (\text{Oligoclase}) \\ &\quad + 0.3FeTiO_3\,(\text{Ilmenite}) + 0.28CO_2 + 1.87SiO_2 + 0.33H_2O \\ &\quad + 0.32Na_2O\ (\text{goes into paragonite in mica}) + 0.33O_2 \end{aligned} \quad (2)$$

This reaction consumes no more than 10% of the calcite or graphite present and liberates 4.2 mmols (0.18 g) of CO_2 per 100 g of rock (Table 2).

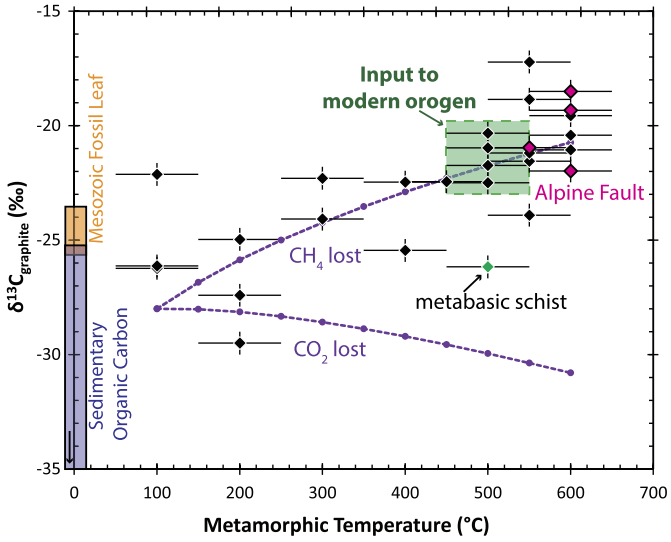

Fig. 4. Measured graphite $\delta^{13}C$ values versus estimated metamorphic temperature. Rayleigh distillation curves are plotted following Evans et al. (2002): $\delta f = \delta i + 1000(F^{\alpha-1} - 1)$ (1) where, δf is the final and δi initial $\delta^{13}C$ values, F is the mole fraction remaining in the reservoir following removal of components and α is the fluid–rock fractionation factor (CO_2-graphite and graphite-CH_4 fractionation equation from Poulson, 1996). These curves describe the data when approximately 2% of the total carbon is lost as CH_4 every 50 °C. In this model initial carbonaceous material $\delta^{13}C$ values of −28‰ at 100 °C evolve to −20.7‰ at 600 °C, consistent with our measured data, although we note that our data display significant variation. Data highlighted by the box are representative of the isotopic composition of carbon that is going into the modern day orogen and exhumed at amphibolite facies adjacent to the Alpine Fault (pink symbols). Mesozoic fossil leaf data from de Ronde et al. (2001) and sedimentary organic carbon from Rollinson (1993). (For interpretation of the references to color in this figure legend, the reader is referred to the web version of this article.)

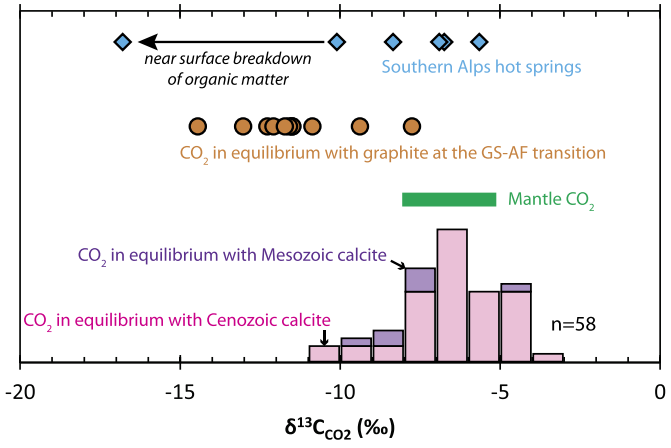

Fig. 5. Comparison of $\delta^{13}C$ values of different carbon reservoirs and outputs in the Southern Alps. $\delta^{13}C$ values of hot spring and CO_2 in equilibrium with Cenozoic calcite (Menzies et al., 2016) and Mesozoic calcite (Templeton et al., 1998), compared with $\delta^{13}C$ value of CO_2 in equilibrium with graphite at the greenschist–amphibolite facies (GS–AF) transition, and mantle CO_2 (Marty and Jambon, 1987).

To calculate the rock mass undergoing greenschist–amphibolite facies metamorphism we consider the geometry of the active orogen:

$$\text{Rock mass/yr} = CR \times T \times L \times \rho_{rock}. \quad (3)$$

A convergence rate (CR) of 0.01 m/yr and a strike length of 100 km (L) for the most active part of the orogen and a 5 km thickness (T) for the region currently undergoing metamorphism and rock density (ρ_{rock}) of 2700 kg/m^3, processes 1.35 × 10^{10} kg/rock/yr. Equation (2) indicates that ~0.18 wt.% of CO_2 is released by calcite decarbonation and the oxidation of graphite during greenschist to amphibolite facies metamorphism, which is equivalent to 2.5 × 10^7 kg/yr (5.7 × 10^8 mol/yr) CO_2 for the Southern Alps orogen.

Alternatively, infiltrating meteoric waters have been suggested as a source of dissolved oxygen to oxidise graphite at relatively low temperatures (~150 °C, Jenkin et al., 1994). However, the calculated $\delta^{13}C$ value of CO_2 generated would be greater than 0‰ which is substantially heavier than $\delta^{13}C$ values measured in warm springs or hydrothermal mineral veins. The ambient redox below the water table is sufficiently low that pyrite is stable and widespread implying that the amount of dissolved oxygen is too low (~ $\log fO_2$ of −45, calculated in Geochemist's Workbench) to permit graphite oxidation. Therefore we discount oxidation of graphite at shallow levels by oxygen dissolved in meteoric waters as a source of CO_2 in the orogen. In addition, the oxidation of carbonaceous material in the surficial weathering environment is also discounted as a CO_2 source since there is limited weathering of eroded carbonaceous material with no oxidation rinds on clasts due to short residence times (Nibourel et al., 2015).

4.3. Composition of crustal fluids and total CO_2 flux to the near surface

The greenschist to amphibolite facies metamorphism results in a whole rock loss of total volatiles of ~1 wt.% (Pitcairn et al., 2006) equating to 1.35 × 10^8 kg/yr of volatiles. When combined with our mass balance calculations (Section 4.2) this yields a fluid containing ~7.5 mol.% CO_2, similar to fluid inclusions in metamorphic quartz veins (~5 mol.%, Craw and Norris, 1993). There is a minor mantle CO_2 flux from the hangingwall directly adjacent (~1 km) to the Alpine Fault of 2 × 10^7 mol/yr (Menzies et al., 2016) and including this gives a total deep flux of 5.9 × 10^8 mol/yr CO_2. However, because Southern Alps hot springs have HCO_3^-/Ca^{2+} ratios of ~9 this indicates that in addition to eq. (2) there must be a minor (~10%) component of calcite dissolution either at depth, or at shallow levels in the active geothermal system (<150 °C). Hence the total CO_2 flux is 6.4 × 10^8 mol/yr, of which 87% is sourced from metamorphic graphite oxidation (25%) and decarbonation of calcite (62%) at the greenschist to amphibolite facies transition, with ~10% from the shallow congruent dissolution of calcite, and 3% mantle-derived.

4.4. CO_2 flux to the atmosphere

The flux calculated in sections 4.2 and 4.3 quantifies the amount of carbon released into the near surface environment. To estimate the flux of CO_2 to the atmosphere from this reservoir, it is necessary to quantify the proportion of CO_2 degassed from geothermal waters (Becker et al., 2008; Evans et al., 2008). We use measured $\delta^{13}C$ values of both DIC and CO_2 from two hot springs and combine these data with carbon isotopic fractionation factors from Mook et al. (1974) for HCO_3–$CO_{2(g)}$ and Rayleigh fractionation modelling combined with a Monte Carlo approach to estimate the likely proportion of CO_2 gas that is lost to the atmosphere from upwelling and effusing hydrothermal waters. In the Monte Carlo simulation, the proportion of CO_2 degassed at each temperature step was randomly generated between 0 and 10% over 1000 iterations of the model. This approach enabled exploration of the range in possible degassing scenarios as the spring waters cool and upwell that result in the measured HCO_3 concentrations, and $\delta^{13}C_{CO_2}$ and $\delta^{13}C_{DIC}$ values (Fig. 6). From these simulations we are able to give realistic maximum and minimum proportions of dissolved CO_2 degassed at each spring. The calculations are constrained by $\delta^{13}C_{CO_2}$ values of −8.8‰ and $\delta^{13}C_{DIC}$ values of −3.6‰ and −4.8‰ for Fox Spring; and $\delta^{13}C_{CO_2}$ values of −7.2‰ and $\delta^{13}C_{DIC}$ values of −4.9‰ and −5.9‰ for Copland Spring (Menzies et al., 2016). The difference in DIC values between the springs, and differences

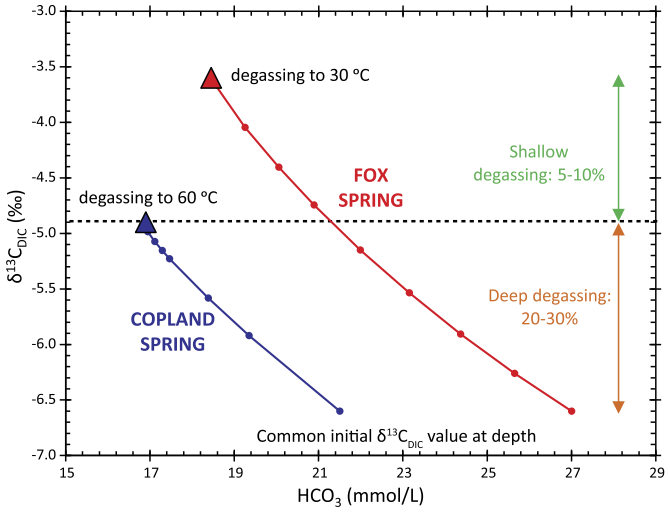

Fig. 6. Rayleigh distillation models of CO_2 degassing during cooling of geothermal waters at two hot springs in the Southern Alps. These models indicate that between 20% and 30% of CO_2 is degassed by 60 °C and a further 5–10% during cooling to 30 °C. Common initial $\delta^{13}C_{DIC}$ value at depth is taken from the average $\delta^{13}C_{HCO_3}$ value calculated from carbonate veins in this area (Menzies et al., 2016). Dots represent proportion degassed and triangles are the final measured $\delta^{13}C_{DIC}$ of each spring.

between CO_2 and DIC $\delta^{13}C$ values is likely due to temperature differences between the spring waters; Fox is ~30–40 °C and Copland ~60 °C at the surface, and isotopic fractionation factors are higher at lower temperatures (Becker et al., 2008). Silica geothermometry suggests these spring waters equilibrated with rock at ~120 °C (Menzies et al., 2016).

The model predicts that for Fox Spring degassing while cooling from 120 to 40 °C results in a net difference between DIC and CO_2 $\delta^{13}C$ values of 5.2‰. This corresponds to degassing of 30 to 50% of the total CO_2 during upwelling, with the higher values representing greater degassing at depth owing to smaller fractionation factors at higher temperatures. For Copland Spring the net difference between DIC and CO_2 $\delta^{13}C$ values is smaller, 2.3‰, which may be obtained through 20–30% degassing. Our data indicate that there is greater fractionation at Fox Spring, and it is unlikely that the differences in $\delta^{13}C$ values of DIC between the springs, and consequently their degassing history, is anything other than temperature-related. This indicates that greater degassing has occurred at Fox Spring, at lower temperatures, and that both fluids shared a similar deep fluid history with degassing between 20–30% followed by a further 10–20% degassing at lower temperatures at Fox Spring. Copland Spring has deposited a large travertine terrace during degassing of CO_2 at the surface indicating that further CO_2 loss occurs after it reaches the surface and it likely releases >20–30% of its initial total dissolved CO_2 to the atmosphere.

Using these estimates, between 30–50% of mantle and metamorphic CO_2 carried in hydrothermal fluids as dissolved CO_2 is liberated as CO_2 gas to the atmosphere, and the rest is added to the riverine HCO_3^- budget. It is likely that there is further, limited degassing of such fluids as they flow to join the rivers, but given our wide range in estimated proportion of degassing we assume it is accounted for within this range. This allows us to revise our mountain belt CO_2 flux to the atmosphere from metamorphic and mantle sources to 1.9 to 3.2 $\times$ 10^8 mol/yr over a 10 $\times$ 100 km area (1.9 to 3.2 $\times$ 10^5 mol/km^2/yr). For comparison the flux of metamorphic CO_2 to the atmosphere from the Himalaya is estimated at 0.9 $\times$ 10^{12} mol/yr over a 2500 $\times$ 300 km area (1.2 $\times$ 10^6 mol/km^2/yr) (Becker et al., 2008), an order of magnitude greater than the Southern Alps. The Southern Alps CO_2 flux calculated here is similar to the lower range of greenschist facies metamorphic CO_2 fluxes (0.5 to 7 $\times$ 10^6 mol/km^2/yr) modelled from carbonation reaction textures in the predominantly siliciclastic Dalradian metasedimentary belt in the SW Scottish Highlands (Skelton, 2011).

4.5. CO_2 drawdown by weathering processes

To estimate the overall influence of Southern Alps orogenesis on the global atmospheric CO_2 budget we compare our estimated CO_2 flux to the atmosphere (Section 4.4) with the estimated short term rates of CO_2 drawdown during silicate and carbonate chemical weathering (Fig. 7, Table 3). Major ion concentrations of rivers draining to the west of the Main Divide have total, short term atmospheric CO_2 consumption rates of 7.5 to 39 $\times$ 10^5 mol/km^2/yr (Table 3, S1 following Jacobson and Blum (2003)). Relatively high Ca/Ca+Mg+Na indicates that carbonate dissolution is the dominant chemical weathering reaction (4.2 to 31 $\times$ 10^5 mol/km^2/yr). The carbonate that contributes to this weathering flux is likely sourced from disseminated carbonate veins that were deposited from hydrothermal fluids at depth, similar to what has been observed in the Himalaya (Blum et al., 1998). This is accompanied by silicate weathering (1.1 to 7.4 $\times$ 10^5 mol/km^2/yr) at rates similar to or up to an order of magnitude higher than the global mean silicate weathering rate (9 $\times$ 10^4 mol/km^2/yr, Table 3). In contrast, rivers draining to the east of the Main Divide have silicate chemical weathering rates of 0.5 to 1.3 $\times$ 10^5 mol/km^2/yr (Jacobson and Blum, 2003), similar to global mean weathering rates. An additional carbon sink is the burial of particulate organic carbon exported from the mountain belt by rivers to the ocean which is estimated at 32.5 mol/km^2/yr and 10% of this is estimated to be stored in marine sediments on geological timescales (Hilton et al., 2008).

High rates of mechanical erosion in the Southern Alps due to rugged relief and orographic precipitation occur over a ~200 km region parallel to the Alpine Fault that extends 25 km east to the Main Divide (Jacobson and Blum, 2003). This is larger than the ~100 $\times$ 10 km region of modern convergence-related metamorphism in the most rapidly uplifting portion of the Alpine Fault hangingwall, that includes numerous warm springs that are effusing CO_2 to the atmosphere (Fig. 1). For this extended region west of the Main Divide the short term weathering drawdown is 0.3 to 2 $\times$ 10^{10} mol/yr of which 5.5 to 37 $\times$ 10^8 mol/yr is due to silicate weathering. This is two to ten times higher than the orogenic flux of CO_2 from the mountain belt to the atmosphere (1.9 to 3.2 $\times$ 10^8 mol/yr).

In the Himalaya CO_2 drawdown by chemical weathering is a factor of three lower than the estimated metamorphic output and therefore the Himalaya is a net source for atmospheric CO_2 (Becker et al., 2008). In contrast, in the Southern Alps CO_2 consumption by weathering is greater than CO_2 production, indicating that orogenic belts with low proportions of carbonate rocks may be CO_2 sinks. As a consequence, major continental collision events through geological time that involved dominantly siliciclastic rocks deposited before the widespread occurrence of marine carbonate sediments (Early Proterozoic, Ronov, 1964) may have been net sinks for CO_2 and had the opposite influence to the modern Himalaya that dominates the modern carbon cycle (Bickle, 1996).

5. Conclusions

1. The Southern Alps is a low carbon siliciclastic mountain belt developed along the transcurrent Australian Pacific plate boundary with modern uplift, metamorphism and hydrothermal activity that is mobilising carbon.
2. Hot spring $HCO_3^-/Ca^{2+} = 9$ which is substantially higher than expected for the dissolution of calcite (1–2), indicating the op-

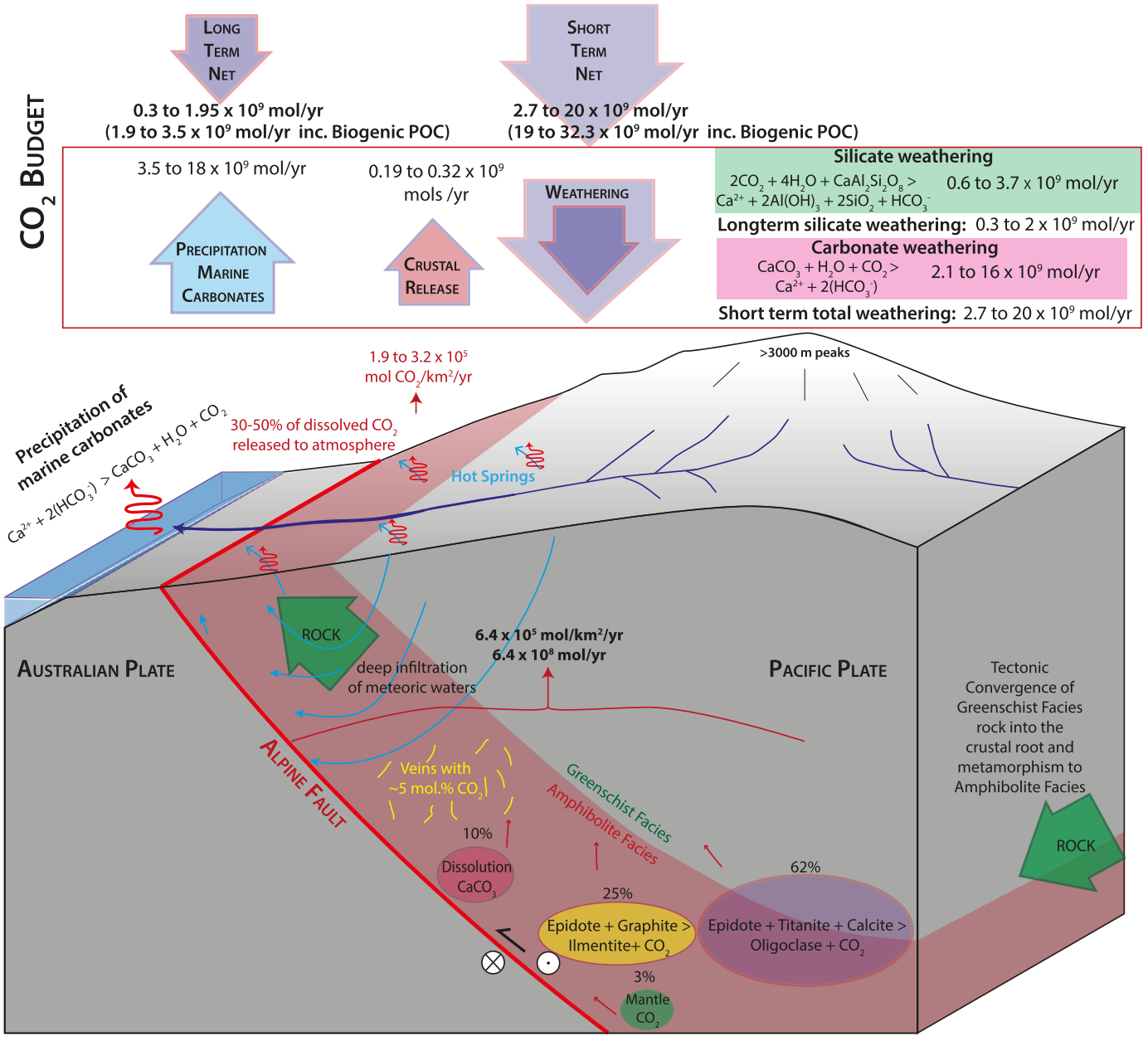

Fig. 7. Summary of the processes generating CO_2 in the Southern Alps orogen compared with rates of CO_2 drawdown through weathering reactions driven by elevated topography and associated enhanced erosion rates. Over short time scales the Southern Alps are a significant sink for CO_2 through weathering reactions, and even when considering long timescales where precipitation of marine carbonates may occur the mountain belt still acts as a net CO_2 sink.

eration of CO_2 producing and/or Ca^{2+} consuming reactions in the subsurface.

3. There are three active principal sources of CO_2: oxidation of graphite and decarbonation of calcite at the greenschist-amphibolite facies boundary (T and P), and dissolution of rock mass calcite at shallower levels. There is only a minor component of mantle CO_2 coming up the Alpine Fault.
4. The total CO_2 flux to the near surface environment is 6.4×10^8 mol/yr, of which 87% is sourced from graphite (25%) and decarbonation of calcite (62%) at the greenschist to amphibolite facies transition, 10% is from congruent dissolution of calcite, and 3% is mantle-derived.
5. The CO_2 flux to the atmosphere from degassing of hot springs is 1.9 to 3.2×10^8 mol/yr, which is 30–50% of the flux to the near surface environment. The balance ($3.2–4.5 \times 10^8$ mol/yr) is either precipitated in subsurface veins, travertine terraces or flows into the river system as a minor component (<1–10%) of the dissolved HCO_3^-.
6. Rapid uplift and orographic precipitation in the Southern Alps enhances mechanical erosion, the comminution of rocks, and exposure of new reactive surface area leading to elevated rates of chemical weathering. The drawdown of CO_2 through this weathering ranges between 2.7 and 20×10^9 mol/yr, which is at least an order of magnitude greater than the CO_2 flux to the atmosphere from the orogenic belt. In addition the rapid removal of particulate organic carbon from the mountain belt removes a further 16.3×10^9 mol/yr of carbon (Hilton et al., 2008).
7. Although graphite oxidation and associated coupled decarbonation processes described above are also likely to occur in carbonate-rich orogens, decarbonation of limestone overwhelmingly dominates CO_2 production in these systems. Siliciclastic mountain belts such as the Southern Alps of New

Table 3
Summary of CO_2 drawdown through silicate and carbonate weathering, and export of particulate organic carbon (POC) from west of the Main Divide in the Southern Alps and total short term drawdown (silicate + carbonate + POC) and total long-term effective drawdown (half of silicate weathering + 10% of POC) compared with crustal CO_2 generation and of that CO_2 which reaches the atmosphere.

		Area (km^2)	$CO_2 \times 10^5$ ($mol/km^2/yr$)	$CO_2 \times 10^9$ (mol/yr)
Silicate Weathering, west of the Main Divide	max	5000	7.4	3.70
	min	5000	1.1	0.55
Carbonate Weathering, west of the Main Divide	max	5000	31	16
	min	5000	4.2	2.1
Biogenic POC, west of the Main Divide		5000	32.5	16.3
Total Short-term drawdown	max	5000	67.5	**32.3**
	min	5000	37.8	**19**
Total Long-term drawdown	max	5000	6.95	**3.5**
	min	5000	3.8	**1.9**
Metamorphic CO_2 generation		1000	6.4	0.64
Metamorphic CO_2 reaching atmosphere	max	1000	3.2	**0.32**
	min	1000	1.9	**0.19**

Zealand, are net sinks for atmospheric CO_2, in contrast to orogens involving abundant carbonate rocks, such as the Himalaya, that are net CO_2 sources.

Acknowledgements

C.D.M. was supported by NERC CASE PhD studentship award NE/G524160/1 (GNS Science, NZ, CASE partner). D.A.H.T. acknowledges support from research grants NE/H012842/1 and NE/J022128/1 and a Royal Society Wolfson Research Merit Award (WM130051). S.C.C. was funded under GNS Science's "Impacts of Global Plate Tectonics in and around New Zealand Programme" (PGST Contract CO5X0203). J.C.A. was supported by NSF OCE 1334758. We also thank Matthew Cooper, Andy Milton, Darryl Green and Lora Wingate for laboratory assistance. We thank Mike Bickle for editorial advice and comments, and reviews from two anonymous reviewers that improved this manuscript.

Appendix A. Supplementary material

Supplementary material related to this article can be found online at https://doi.org/10.1016/j.epsl.2017.10.010.

References

Barnes, I., Downes, C.J., Hurlston, J.R., 1978. Warm Springs, South Island New Zealand and their potentials to yield Laumontite. Am. J. Sci. 278, 1412–1427.
Becker, J.A., Bickle, M.J., Galy, A., Holland, T.J.B., 2008. Himalayan metamorphic CO_2 fluxes: quantitative constraints from hydrothermal springs. Earth Planet. Sci. Lett. 265, 616–629.
Beyssac, O., Cox, S.C., Vry, J., Herman, F., 2016. Peak metamorphic temperature and thermal history of the Southern Alps (New Zealand). Tectonophysics.
Bickle, M.J., 1996. Metamorphic decarbonation, silicate weathering and the long-term carbon cycle. Terra Nova 8, 270–276.
Blum, J.D., Gazis, C.A., Jacobson, A.D., Chamberlain, C.P., 1998. Carbonate versus silicate weathering in the Raikhot watershed within the High Himalayan Crystalline Series. Geology 26, 411–414.
Boese, C.M., Townend, J., Smith, E., Stern, T., 2012. Microseismicity and stress in the vicinity of the Alpine Fault, central Southern Alps, New Zealand. J. Geophys. Res., Solid Earth 117, B02302.
Bottinga, Y., 1968. Calculation of fractionation factors for carbon and oxygen isotopic exchange in the system calcite–carbon dioxide–water. J. Phys. Chem. 72, 800–808.
Brady, P.V., 1991. The effect of silicate weathering on global temperature and atmospheric CO_2. J. Geophys. Res., Solid Earth 96, 18101–18106.
Cox, S.C. Barrell, D.J.A., 2007. Geology of the Aoraki area. Institute of Geological and Nuclear Sciences 1:250 000 geological map 15. 1 sheet + 71 p. Lower Hutt, New Zealand. GNS Science.
Cox, S.C., Menzies, C.D., Sutherland, R., Denys, P.H., Chamberlain, C., Teagle, D.A.H., 2015. Changes in hot spring temperature and hydrogeology of the Alpine Fault hanging wall, New Zealand, induced by distal South Island earthquakes. Geofluids 15, 216–239.
Cox, S.C., Sutherland, R., 2007. Regional geological framework of South Island, New Zealand, and its significance for understanding the active plate boundary. In: Okaya, D., Stern, T., Davey, F. (Eds.), A Continental Plate Boundary: Tectonics at South Island, New Zealand. American Geophysical Union, Washington, DC, pp. 19–46.
Craw, D., Norris, R.J., 1993. Grain boundary migration of water and carbon dioxide during uplift of garnet-zone Alpine Schist, New Zealand. J. Metamorph. Geol. 11, 371–378.
de Ronde, C.E.J., Sibson, R.H., Bray, C.J., Faure, K., 2001. Fluid chemistry of veining associated with an ancient microearthquake swarm, Benmore Dam, New Zealand. Geol. Soc. Am. Bull. 113, 1010–1024.
Evans, K.A., Bickle, M.J., Skelton, A.D.L., Hall, M., Chapman, H., 2002. Reductive deposition of graphite at lithological margins in East Central Vermont: a Sr, C and O isotope study. J. Metamorph. Geol. 20, 781–798.
Evans, M.J., Derry, L.A., France-Lanord, C., 2008. Degassing of metamorphic carbon dioxide from the Nepal Himalaya. Geochem. Geophys. Geosyst. 9.
Gaillardet, J., Dupré, B., Louvat, P., Allègre, C.J., 1999. Global silicate weathering and CO_2 consumption rates deduced from the chemistry of large rivers. Chem. Geol. 159, 3–30.
Galy, A., France-Lanord, C., 1999. Weathering processes in the Ganges–Brahmaputra basin and the riverine alkalinity budget. Chem. Geol. 159, 31–60.
Grapes, R., Otsuki, M., 1983. Peristerite compositions in quartzofeldspathic schists, Franz Josef–Fox Glacier area, New Zealand. J. Metamorph. Geol. 1, 47–61.
Grapes, R., Watanabe, T., 1992. Metamorphism and uplift of Alpine schist in the Franz Josef–Fox Glacier area of the Southern Alps, New Zealand. J. Metamorph. Geol. 10, 171–180.
Henne, A., Craw, D., 2012. Synmetamorphic carbon mobility and graphite enrichment in metaturbidites as a precursor to orogenic gold mineralisation, Otago Schist, New Zealand. Miner. Depos. 47, 781–797.
Hilton, R.G., Galy, A., Hovius, N., 2008. Riverine particulate organic carbon from an active mountain belt: importance of landslides. Glob. Biogeochem. Cycles 22, 12.
Hu, S., Evans, K., Craw, D., Rempel, K., Bourdet, J., Dick, J., Grice, K., 2015. Raman characterization of carbonaceous material in the Macraes orogenic gold deposit and metasedimentary host rocks, New Zealand. Ore Geol. Rev. 70, 80–95.
Jacobson, A.D., Blum, J.D., 2003. Relationship between mechanical erosion and atmospheric CO_2 consumption in the New Zealand Southern Alps. Geology 31, 865–868.
Jacobson, A.D., Blum, J.D., Chamberlain, C.P., Craw, D., Koons, P.O., 2003. Climatic and tectonic controls on chemical weathering in the New Zealand Southern Alps. Geochim. Cosmochim. Acta 67, 29–46.
Jenkin, G.R.T., Craw, D., Fallick, A.E., 1994. Stable isotopic and fluid inclusion evidence for meteoric fluid penetration into an active mountain belt: Alpine Schist, New Zealand. J. Metamorph. Geol. 12, 429–444.
Kelemen, P.B., Manning, C.E., 2015. Reevaluating carbon fluxes in subduction zones, what goes down, mostly comes up. Proc. Natl. Acad. Sci. USA 112, E3997–E4006.
Kerrick, D.M., McKibben, M.A., Seward, T.M., Caldeira, K., 1995. Convective hydrothermal CO_2 emission from high heat flow regions. Chem. Geol. 121, 285–293.
Kirilova, M., Toy, V.G., Timms, N., Halfpenny, A., Menzies, C.D., Craw, D., Beyssac, O., Sutherland, R., Townend, J., Boulton, C.J., Carpenter, B.M., Cooper, A.F., Grieve, J., Little, T.A., Morales, L., Morgan, C., Mori, H., Schleicher, A., Williams, J., in press.

Textural changes of graphitic carbon by tectonic and hydrothermal processes in an active plate boundary fault zone, Alpine Fault, New Zealand. Geol. Soc. (Lond.) Spec. Publ. 453. https://doi.org/10.1144//SP453.13.

Könitzer, S.F., Leng, M.J., Davies, S.J., Stephenson, M.H., 2012. An assessment of geochemical preparation methods prior to organic carbon concentration and carbon isotope ratio analyses of fine-grained sedimentary rocks. Geochem. Geophys. Geosyst. 13.

Koons, P.O., 1987. Some thermal and mechanical consequences of rapid uplift: an example from the Southern Alps, New Zealand. Earth Planet. Sci. Lett. 89, 307–319.

Koons, P.O., 1989. The topographic evolution of collisional mountain belts: a numerical look at the Southern Alps, New Zealand. Am. J. Sci. 289, 1041–1069.

Marty, B., Jambon, A., 1987. $C/^3He$ in volatile fluxes from the solid Earth: implications for carbon geodynamics. Earth Planet. Sci. Lett. 83, 16–26.

Menzies, C.D., Teagle, D.A.H., Craw, D., Cox, S.C., Boyce, A.J., Barrie, C.D., Roberts, S., 2014. Incursion of meteoric waters into the ductile regime in an active orogen. Earth Planet. Sci. Lett. 399, 1–13.

Menzies, C.D., Teagle, D.A.H., Niedermann, S., Cox, S.C., Craw, D., Zimmer, M., Cooper, M.J., Erzinger, J., 2016. The fluid budget of a continental plate boundary fault: quantification from the Alpine Fault, New Zealand. Earth Planet. Sci. Lett. 445, 125–135.

Mook, W.G., Bommerson, J.C., Staverman, W.H., 1974. Carbon isotope fractionation between dissolved bicarbonate and gaseous carbon dioxide. Earth Planet. Sci. Lett. 22, 169–176.

Mortimer, N., 2004. New Zealand's geological foundations. Gondwana Res. 7, 261–272.

Nibourel, L., Herman, F., Cox, S.C., Beyssac, O., Lavé, J., 2015. Provenance analysis using Raman spectroscopy of carbonaceous material: a case study in the Southern Alps of New Zealand. J. Geophys. Res., Earth Surf. 120, 2056–2079.

Norris, R.J., Cooper, A.F., 2007. The Alpine Fault, New Zealand: surface geology and field relations. In: Okaya, D., Stern, T., Davey, F. (Eds.), A Continental Plate Boundary: Tectonics at South Island, New Zealand. American Geophysical Union, Washington, DC, pp. 157–175.

Pitcairn, I.K., 2004. Sources of Fluids and Metals in Orogenic Gold Deposits: The Otago Schists, New Zealand. Faculty of Science, School of Ocean and Earth Sciences, University of Southampton, Southampton.

Pitcairn, I.K., Craw, D., Teagle, D.A.H., 2014. The gold conveyor belt: large-scale gold mobility in an active orogen. Ore Geol. Rev. 62, 129–142.

Pitcairn, I.K., Roberts, A., Teagle, D.A.H., Craw, D., 2005. Detecting hydrothermal graphite deposition during metamorphism and gold mineralisation. J. Geol. Soc. Lond. 162, 429–432.

Pitcairn, I.K., Teagle, D.A.H., Craw, D., Olivio, G.R., Kerrich, R., Brewer, T.S., 2006. Sources of metals and fluids in orogenic gold deposits: insights from the Otago and Alpine Schists, New Zealand. Econ. Geol. 101, 1525–1546.

Poulson, S.R., 1996. Equilibrium mineral–fluid stable isotope fractionation factors in graphitic metapelites. Chem. Geol. 131, 207–217.

Raymo, M.E., Ruddiman, W.F., 1992. Tectonic forcing of late Cenozoic climate. Nature 359, 117–122.

Rollinson, H.R., 1993. Using Geochemical Data: Evaluation, Presentation, Interpretation. Longman Scientific and Technical. Copublished in the U.S. with J. Wiley and Sons, Harlow, Essex, England, New York.

Ronov, A.B., 1964. Common tendencies in the chemical evolution of the Earth's crust, ocean, and atmosphere. Geochem. Int. 4, 713–737.

Skelton, A., 2011. Flux rates for water and carbon during greenschist facies metamorphism. Geology 39, 43–46.

Sutherland, R., Davey, F., Beavan, J., 2000. Plate Boundary deformation in South Island, New Zealand, is related to inherited lithospheric structure. Earth Planet. Sci. Lett. 177, 141–151.

Sutherland, R., Toy, V.G., Townend, J., Cox, S.C., Eccles, J.D., Faulkner, D.R., Prior, D.J., Norris, R.J., Mariani, E., Boulton, C., Carpenter, B.M., Menzies, C.D., Little, T.A., Hasting, M., De Pascale, G.P., Langridge, R.M., Scott, H.R., Reid-Lindroos, Z., Fleming, B., Kopf, A.J., 2012. Drilling reveals fluid control on architecture and rupture of the Alpine Fault, New Zealand. Geology 40, 1143–1146.

Teagle, D.A.H., Hall, C.M., Cox, S.C., Craw, D., 1998. Ar/Ar dating and uplift rate of hydrothermal minerals in the Southern Alps, New Zealand. Water-Rock Interact. 9, 801–804.

Templeton, A.S., Chamberlain, C.P., Koons, P.O., Craw, D., 1998. Stable isotopic evidence for mixing between metamorphic fluids and surface-derived waters during recent uplift of the Southern Alps, New Zealand. Earth Planet. Sci. Lett. 154, 73–92.

Upton, P., Craw, D., Yu, B., Chen, Y.-G., 2011. Controls on fluid flow in transpressive orogens, Taiwan and New Zealand. Geol. Soc. (Lond.) Spec. Publ. 359, 249–265.